J. Fluid Mech. (1980), *vol.* 99, *part* 3, *pp.* 655–672
Printed in Great Britain

Mean flows driven by weak eddies in rotating systems

By A. D. McEWAN, R. O. R. Y. THOMPSON† AND R. A. PLUMB
CSIRO Division of Atmospheric Physics, Aspendale, Victoria, 3195, Australia

(Received 1 August 1979 and in revised form 8 January 1980)

General relations are derived for the forcing of a mean zonal flow in a damped rotating barotropic system through the action of weak eddies. In particular it is found that if the eddies are forced at localized latitudes the induced motion away from these latitudes is likely to be counter to the rotation (i.e. 'easterly'). Over the forcing latitude the mean motion is always westerly except when the forcing provides a sink of relative momentum. In the case when the background field is deformed topographically to generate eddies the divergence of the Reynolds stress is balanced at lowest order by a dynamic pressure drag, and the mean motion takes the direction of propagation of the forcing.

The relations are applied to a linearized Rossby wave field in a viscous fluid driven by a moving system of boundary sources and sinks or hills and hollows. The results are compared with laboratory experiments. All major predictions are confirmed qualitatively, but the discrepancies in detail indicate the influence of nonlinear effects other than those incorporated in the theory.

1. Introduction

There is abundant observational evidence (e.g. Oort & Rasmussen 1971; Newell *et al.* 1972; Holopainen 1978; Blackmon *et al.* 1977) that the synoptic-scale eddy components of the atmosphere's motion play an important role in transporting horizontal momentum on both global and regional scales, usually with the effect of enhancing the zonal mean circulation at mid-latitudes. In the ocean similar effects on a smaller scale have been observed in relation to the Gulf Stream where the boundary eddies induce a westerly momentum convergence on the stream and a corresponding easterly flow beyond it (Webster 1965; Thompson 1977, 1978).

The eddy contribution arises from Reynolds stress terms in the horizontal mean momentum equation, implying that in a rotationally dominated field the eddies acquire a structure or orientation which enables them to transfer momentum in a preferred direction, in many cases opposing the gradient of mean relative momentum.

Although this counter-gradient property seemed at first remarkable enough to earn Starr's (1968) evocative title of 'negative viscosity', it can be explained for quasi-geostrophic motions at least by simple consideration of the effects of eddy vorticity transport, and indeed offers a vindication of Taylor's (1915) vorticity-diffusion hypothesis. Held (1975) and Rhines & Holland (1979) noted that growing eddy intensity and dissipation at constant intensity each imply a down-gradient flux of

† Present address: CSIRO Division of Fisheries & Oceanography, Cronulla, N.S.W. 2230, Australia.

eddy potential vorticity and an easterly forcing of the mean zonal motion (q.v., equations (2.5) and (2.7)) in regions when the eddies themselves are unforced. Momentum conservation then implies that in the eddy-forcing regions, if localized, the induced zonal motion is westerly. Earlier, Thompson (1971) had noted that for barotropic Rossby waves the radiation of energy from a localized forcing region implies an oppositely directed flux of westerly momentum; hence if the Gulf Stream were a generator of oceanic eddies it could be intensified by their dispersion.

These effects and general eddy diffusion properties have been discussed for a variety of cases by Rhines & Holland (1979). The predictions generally bear out the results of numerical experiments on barotropic and baroclinic systems (e.g. Lorenz 1960; Hollingsworth 1975; Moura & Stone 1976; Simmons & Hoskins 1976). Global baroclinic models by Baines & Frederiksen (1978) and Frederiksen (1979) indicate the action of the momentum-exchange process on a regional scale.

In view of the evident importance of the topic, surprisingly little has been done in the laboratory on eddy–mean-flow interaction in rotating systems. Whitehead (1975) succeeded in producing a westerly zonal jet bounded by easterly jets by oscillating a small plunger in a large shallow rotating water tank. The localized nature of the forcing made the results unsuitable for detailed evaluation, and Colin de Verdière (1977, 1979) conducted another experiment with regular, zonally periodic forcing in a topographic polar beta-plane simulation. This latter experiment (in fact the progenitor of the source–sink experiments described here) enabled detailed comparisons to be made with theory but unfortunately the location of the forcing region adjacent to the circumference of the experimental vessel prevented the direct measurement of mean flows to this boundary and the presence of a westerly jet in this region could only be inferred.

The present experiments were undertaken with these shortcomings in mind, and were intended to provide continuous, small-amplitude, localized forcing of a single zonal wavenumber with minimum turbulence. A topographic forcing method was attempted first, and was found to be incapable of generating significant westerly flow. This unexpected result led to a general examination of the problem (§ 2) yielding an explanation and several useful results concerning frictionally damped planetary eddy motions.

A second experimental method was tried in which forcing was provided by a means similar to that used by Colin de Verdière, but with the forcing region separated from the container side walls. Within a range of forcing phase speeds, westerly jets could be induced over the forcing region, bounded on both sides by easterly flow. The results (§ 4) are compared with theoretical predictions for a linear, locally forced Rossby wave (§ 3) and quantitative agreement is obtained. The experiments reveal the strong influence of advection and Doppler shifting (discussed briefly in § 3) in determining the character of rectified flows as their amplitude becomes large.

2. Flow rectification by forced quasi-geostrophic eddies

As a synthesis of the experiments described later we consider uniform fluid of depth h_0 in a rotating Cartesian frame (x eastward, y poleward) subjected to two different kinds of forcing which are approximately sinusoidal in the zonal direction x and localized in y; dissipation occurs through a viscous boundary layer.

The quasi-geostrophic potential vorticity equation is [cf. Stern 1975, equation (5.3.11)]

$$\frac{D}{Dt}\left[\zeta - \frac{fh}{h_0}(x,y,t)\right] = -\frac{f}{h_0}[\delta\zeta - W_0'(x,y,t)]. \tag{2.1}$$

Here f is background vorticity, $\zeta = v_x - u_y$ is relative vorticity, δ is the net thickness of an Ekman layer on the bottom rigid boundary at $z = -(h_0+h)$; W_0' is the normal surface velocity through this boundary if it is porous. Boundary slope and acceleration are assumed to be small and $|W_0'| \leqslant O(f\delta)$. Primes denote quantities whose x and t averages are zero. The system is therefore forced both by periodic variations in depth and by boundary suction or ejection.

Also defined are the linearized potential vorticity

$$q = \zeta - fh/h_0, \tag{2.2}$$

$\lambda = f\delta/h_0$ and $w_0' = fW_0'/h_0$. Separated into zonally averaged and periodic parts, ζ and q are rewritten:

$$\zeta = \bar{\zeta}(y,t) + \zeta'(x,y,t),$$

$$q = \bar{\zeta} - \frac{fh(y)}{h_0} + \zeta' - \frac{fh'(x,y,t)}{h_0};$$

$\bar{q}_y$ is equivalent to 'β' in conventional notation.

Taking the zonal average of (2.1) gives

$$\left[\frac{\partial}{\partial t} + \lambda\right]\bar{\zeta} = -\overline{(v'q')_y}. \tag{2.3}$$

Subtracting, and linearizing the result,

$$q_t' + v'\bar{q}_y + \bar{u}q_x' = -\lambda\zeta' - w_0'. \tag{2.4}$$

Now $\bar{v}_x$ is taken to be zero, so $\bar{\zeta} = -\bar{u}_y$ and providing the disturbances vanish far away from the forcing latitude

$$\left(\frac{\partial}{\partial t} + \lambda\right)\bar{u} = \overline{(v'q')}. \tag{2.5}$$

The zonal driving force per unit volume $\overline{(v'q')}$ is expressible two ways.

(1) by direct expansion, noting that $\overline{(v'^2)}_x$ and $\overline{(u'^2)}_x$ are zero,

$$\overline{(v'q')} = -\overline{(v'u')}_y - f\overline{(v'h')}/h_0 \tag{2.6}$$

where the first right-hand term is mean Reynolds stress divergence and the second term gives the direct contribution of topographic forcing;

(2) taking (2.4), multiplying by q' and averaging

$$\overline{(v'q')} = -\left[\overline{(w_0'q')} + \frac{\partial}{\partial t}\left(\frac{1}{2}\overline{q'^2}\right) + \lambda\overline{(\zeta'q')}\right]/\bar{q}_y \tag{2.7}$$

which then incorporates explicitly the contribution of boundary pumping. The two contributions will be considered separately.

2.1. *Induced motions in unforced regions*

In unforced regions where $w_0' = h' = 0$, $q' = \zeta'$ and substitution of (2.7) into (2.5) gives

$$\left(\frac{\partial}{\partial t}+\lambda\right)\overline{u} = -\frac{1}{\bar{q}_y}\left(\frac{1}{2}\frac{\partial}{\partial t}+\lambda\right)\overline{q'^2}. \tag{2.8}$$

A similar equation was derived by Rhines & Holland (1979). After a time $t \gg \lambda^{-1}$ the flow becomes steady, with

$$\overline{u} = -\frac{1}{\bar{q}_y}\overline{q'^2}. \tag{2.9}$$

This has two important implications; firstly that a zonal mean motion is an intrinsic accompaniment to eddies in a real rotating fluid, and secondly that *away* from the forcing regions, the sign of the motion is necessarily opposite to that of the lateral gradient of potential vorticity. Note that (2.9) should not be taken to imply that $\overline{u} \to \infty$ as $\bar{q}_y \to 0$ since for $\lambda \to 0$,

$$q' \sim -\eta'\bar{q}_y, \tag{2.10}$$

where y' is the radial parcel displacement in the sense defined by Rhines (1977). Therefore (2.9) becomes

$$\overline{u} \sim -\bar{q}_y\overline{\eta'^2}. \tag{2.11}$$

Rhines (1977) arrived at this result and noted that it differed from the corresponding inviscid result (obtained by setting $\lambda = 0$ in (2.8) and integrating from a state of no motion at $t = 0$) by a factor of two. The correspondence, which may seem remarkable in view of the different balance of forces in the two cases, arises because of the similar effects of wave transience and dissipation on wave-mean flow interaction. This similarity, noted by Held (1975) among others, is exemplified by the form of the wave driving term on the right-hand side of (2.8).

Rhines argued that since $\overline{u}$ in the unforced latitudes is easterly (for positive $\bar{q}_y$) momentum conservation requires a westerly jet at the forcing latitude, unless the forcing provides momentum. This condition is satisfied by a source–sink forcing mechanism, but although Whitehead (1975) observed such a jet using a localized kind of topographic forcing it does not follow that the zonally distributed topographic forcing envisaged here would accomplish the same result, since the topography is capable of extracting momentum. This question is examined further below.

2.2. *Topographic forcing*

If the forcing is purely topographic, i.e. $w_0' = 0$, there is associated with the topography a pressure drag per unit area of

$$\overline{(p'h'_x)} = -\overline{(p'_x h')} = -f\overline{(v'h')} \tag{2.12}$$

since $p'_x = fv'$ for quasi-geostrophic flow. Thus the force per unit mass on overlying fluid is $-f\overline{(v'h')}/h_0$. This is transmitted by a mean meridional circulation driven topographically (see McIntyre 1980 for a discussion). Although the Lagrangian mean

vertical velocity of the boundary is zero there exists a non-zero mean vertical velocity in the plane $z = 0$, i.e.

$$\overline{w}(0) = \frac{Dh}{Dt} = \overline{(u'h'_x)} + \overline{(v'h'_y)} = \overline{(v'h')}_y. \tag{2.13}$$

The associated vortex stretching acts to spin up the interior motion.

Now from (2.7) with $w'_0 = 0$ and for steady waves, i.e. $\partial(\overline{q'^2})/\partial t = 0$,

$$\overline{(v'q')} = -\lambda(\overline{\zeta'q'})/q_y,$$

which indicates that as $\lambda \to 0$ the forcing must vanish also. In terms of (2.6) this implies that as $\lambda \to 0$ the divergence of Reynolds stress and the topographic drag cancel *exactly*. This result accords with the 'non-acceleration' theorem as generalized by Andrews & McIntyre (1978); if the shape of the lower boundary remains constant although propagating in x, its Lagrangian mean vertical displacement is zero so according to that theorem there is no mean acceleration for steady conservative waves.

2.3. *Boundary pumping and non-topographic forcing*

When w'_0 is non-zero $\overline{(v'q')}$ and hence $\overline{u}_t$ may remain finite as $\lambda \to 0$. The lower boundary is no longer a material surface and the mean Lagrangian vertical velocity is not necessarily zero there. In a closed system mass conservation requires the Eulerian mean vertical velocity to be zero. However the vertical component of the Stokes drift $\overline{w}^s$ is non-zero but for small-amplitude waves (see Andrews & McIntyre 1978)

$$\overline{w}^s = [\overline{(w'\eta')}_y]_{z=0}. \tag{2.14}$$

When $\lambda \to 0$ and motions are small, (2.4) can be written

$$\left(\frac{\partial}{\partial t} + \overline{u}\frac{\partial}{\partial x}\right)(q' + \eta'\overline{q}_y) = -w'_0,$$

or, with the substitution

$$\left(\frac{\partial}{\partial t} + \overline{u}\frac{\partial}{\partial x}\right) z'_0 = w'_0, \tag{2.15}$$

$$q' + \eta'\overline{q}_y = -z'_0.$$

Equation (2.12) may then be written

$$\overline{w}^s = -[\overline{(w'_0 q')}/\overline{q}_y]_y \tag{2.16}$$

since, from (2.15), $\overline{(w'_0 z'_0)} = 0$ for steady waves. Therefore if $\overline{(w'_0 q')} \neq 0$ the Lagrangian-mean velocity $\overline{w}^L = \overline{w} + \overline{w}^s$ is non-zero at the lower boundary. The conditions of the non-acceleration theorem are thus violated and $\overline{u}_t$ may remain finite as $\lambda \to 0$.

If λ is non-zero (2.5) and (2.7) can be combined to give

$$\lambda\overline{u} \sim -[\overline{(w'_0 q')} + \lambda(\overline{\zeta'q'})]/\overline{q}_y \tag{2.17}$$

for steady waves.

Alternatively, with (2.6) and $h' = 0$,

$$\overline{u} \sim -\frac{1}{\lambda}\overline{(v'u')}_y = -\overline{(v'u')}_y \frac{h_0}{\delta f}, \tag{2.18}$$

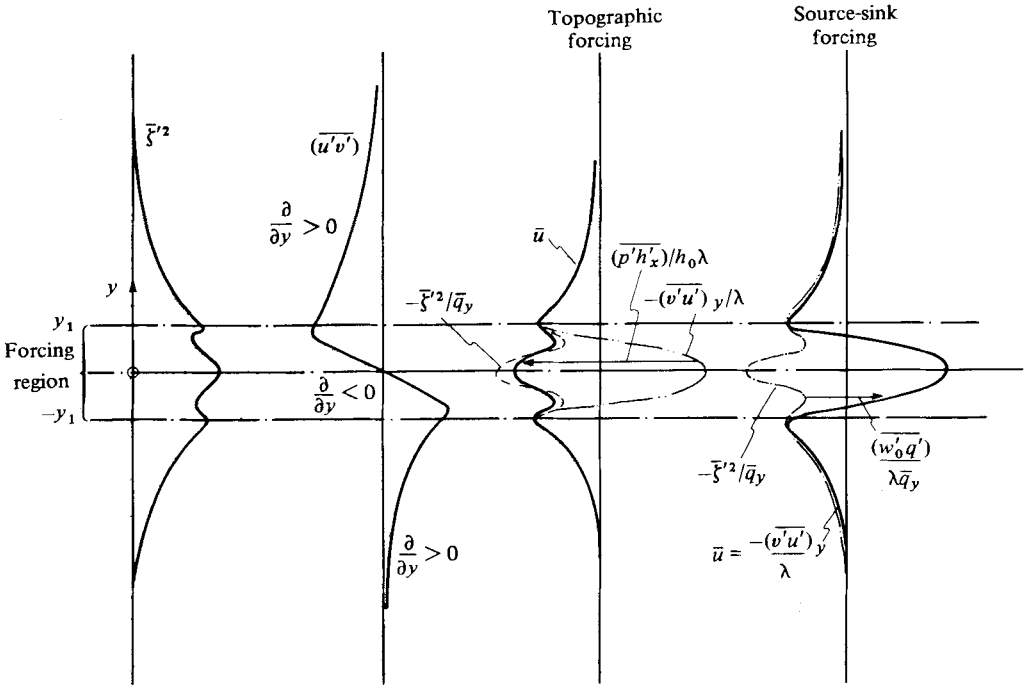

FIGURE 1. Mean-square vorticity, Reynolds stress and mean velocity profiles over an eddy-forcing region located between $-y_1$ and y_1.

where for a viscous laminar medium $\delta = (\nu/2f)^{\frac{1}{2}}$. This last expression effectively expresses the process as a balance between Reynolds stress-driven spin-up and Ekman layer spin-down. The momentum is the amount accumulated by the Reynolds stress in one spin-down time period. The result is directly useful, since it affords a simple means of verification from observational data (see § 4 and figure 11).

Beyond the forcing region (2.2), (2.6) and (2.7) give a general functional relationship between Reynolds stress divergence and mean-square vorticity:

$$\lambda \overline{\zeta'^2} = \bar{q}_y (\overline{v'u'})_y. \tag{2.19}$$

In the system considered $\bar{q}_y$ is positive so $(\overline{v'u'})_y$ is *necessarily* positive in the unforced regions (and $\bar{u}$ is necessarily negative). Furthermore if the forcing is localized to a region $-y_1 < y < y_1$ and the medium is effectively unbounded the eddy amplitude and $|(\overline{v'u'})|$ decay to zero as $|y|$ becomes large. Therefore *within* the forcing region the sign of $(\overline{v'u'})_y$ must be reversed and there must exist a corresponding positive mean flow. Herein lies the essential difference between non-topographic and topographic forcing. With the latter there will also be a reversal in $(\overline{v'u'})_y$ but it is counteracted by the topographic pressure drag. These features are illustrated in figure 1.

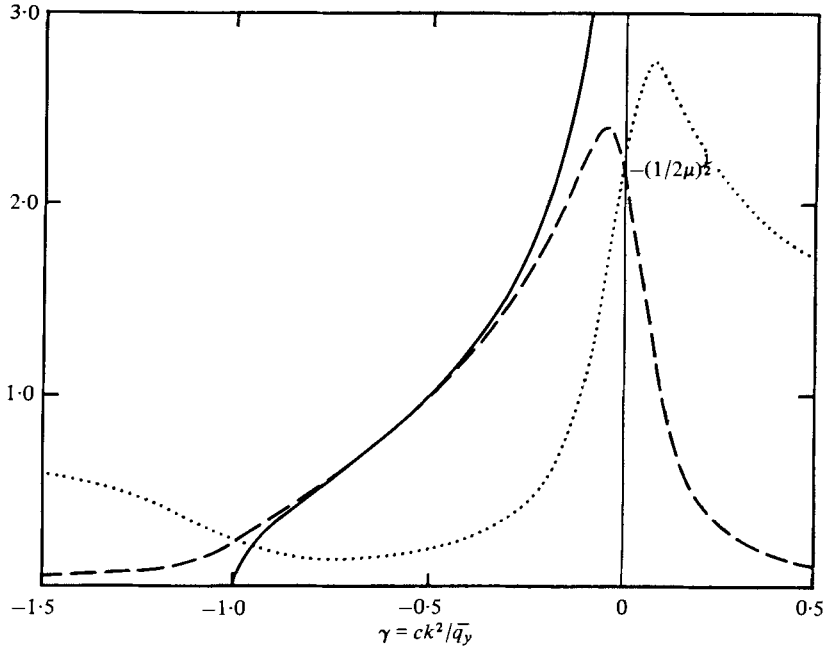

FIGURE 2. Dispersion relation for a damped Rossby wave. ——, l/k without damping; – – –, l/k, $\mu = 0{\cdot}1$; · · · · ·, d/k, $\mu = 0{\cdot}1$.

3. Flows induced by Rossby-wave radiation

The foregoing predictions are given further physical substance by consideration of a simple Rossby-wave field. Neglecting disturbance vorticity advection (2.1) becomes

$$q'_t = -\bar{q}_y v' - \lambda\rho' - w'_0. \tag{3.1}$$

The motion is unbounded in y and forcing is confined within $-y_1 < y < y_1$. The disturbance stream function is written

$$\psi = \mathrm{Re}\,[\psi(y)\, e^{ik(x-ct)}], \tag{3.2}$$

and forcing functions are represented by a half-sinusoid in the y direction:

$$h' = h_0\,\mathrm{Re}\,[H\cos Ly\, e^{ik(x-ct)}], \tag{3.3}$$

$$w'_0 = \mathrm{Re}\,[iW\cos Ly\, e^{ik(x-ct)}], \tag{3.4}$$

where $L = \frac{1}{2}y_1^{-1}\pi$. Substitution in (3.1) gives

$$[1+(i\lambda/ck)]\,[k^{-2}\partial^2/\partial y^2 - 1]\,\psi - (\bar{q}_y/ck^2)\,\psi = F\cos Ly, \tag{3.5}$$

with $F = fH/k^2$ for pure topographic forcing and $F = -W/ck^3$ for pure boundary pumping.

3.1. *Wave dispersion and average mean flow*

In the unforced regions $F = 0$ and an appropriate solution to (3.5) for $y > y_1 > 0$ is

$$\psi = Ae^{i(l+id)y} \tag{3.6}$$

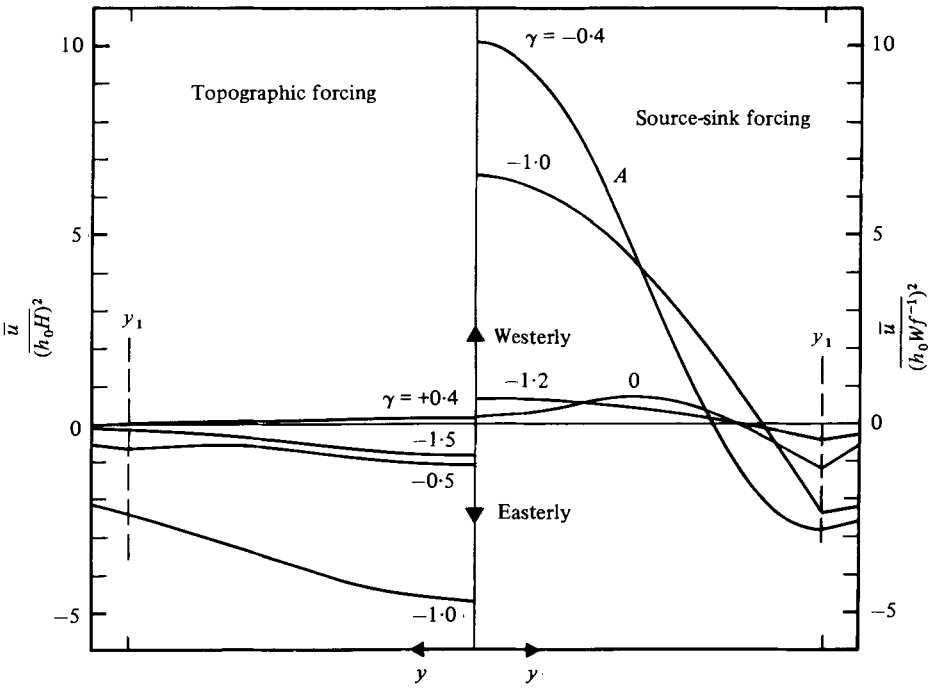

FIGURE 3. Profiles of mean zonal velocity over forcing region for topographic forcing (to the left of central axis) and source sink forcing (to the right).

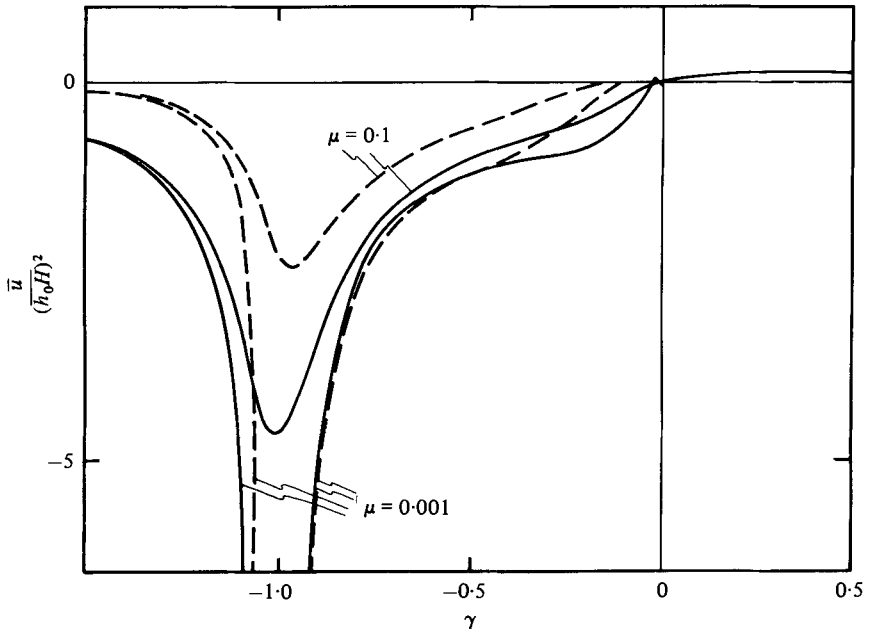

FIGURE 4. Zonal jet strength showing dependence on phase-speed parameter γ, for topographic forcing. ——, velocity on forcing axis, $\bar{u}(y = 0)$; – – –, velocity at edge of forcing region, $\bar{u}(y = y_1)$. For these results, k, L, f, $\bar{q}_y$ and h_0 equal 1. Velocities are scaled by the square of maximum disturbance h'.

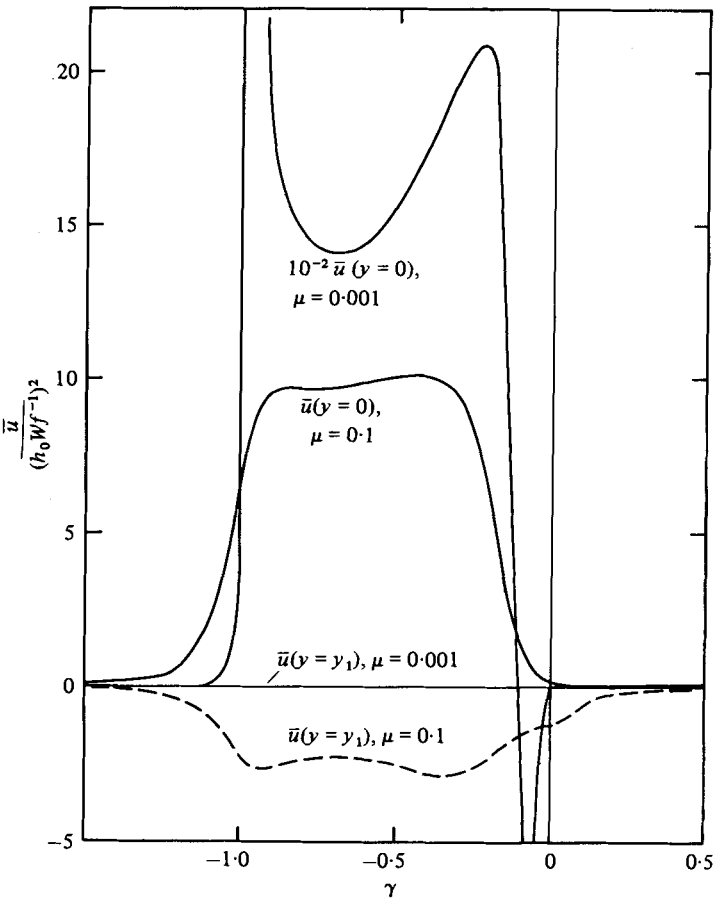

FIGURE 5. As for figure (4) but with source sink forcing. Velocities are scaled by the square of the maximum disturbance vertical velocity W_0'.

where

$$l^2 = \tfrac{1}{2}[\epsilon + (\epsilon^2 + 4\alpha^2)^{\frac{1}{2}}], \tag{3.7}$$

and $d = \alpha/l$,

with $\alpha = \tfrac{1}{2}k^2\mu(\gamma^2+\mu^2)^{-1}$, $\epsilon = -k^2(\gamma^2+\mu^2+\gamma)(\gamma^2+\mu^2)^{-1}$,

and where $\gamma = ck^2/\bar{q}_y$ is the forcing phase-speed parameter,

$\mu = \lambda k/\bar{q}_y$ is the damping parameter.

In the inviscid limit ($\mu \sim 0$) these expressions reduce to the simple dispersion relation for Rossby waves,

$$l_0 = l(\mu = 0) = k[-(1+\gamma^{-1})]^{\frac{1}{2}} \tag{3.8}$$

yielding real, radiating modes (l real) only while $-1 < \gamma < 0$. If μ is non-zero (damping finite) l and d are non-singular and for μ small, both intersect the $\gamma = 0$ axis at about $(k^2/2\mu)^{\frac{1}{2}}$. Figure 2 shows l/k and d/k for $\mu = 0$ and $\mu = 0{\cdot}1$.

Substitution of (3.6) and (3.7) in (2.18) gives the terminal mean-flow profile beyond the forcing region:

$$\bar{u}(y > y_1) = -\tfrac{1}{2}k^4|A|^2\bar{q}_y^{-1}(\gamma^2+\mu^2)^{-1}\,e^{-2dy}. \tag{3.9}$$

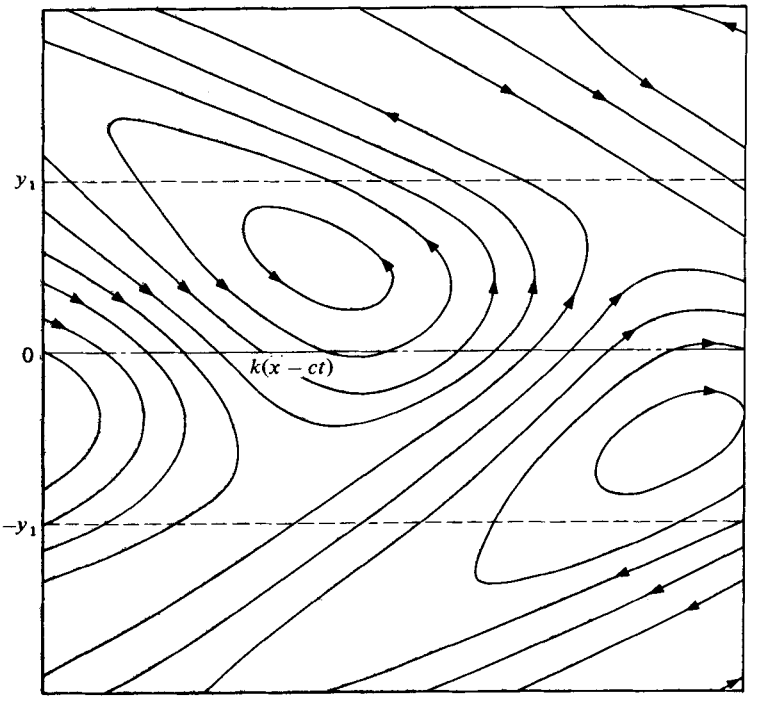

FIGURE 6. New streamlines (disturbance plus induced mean flow) for condition of curve *A*, figure 3, with $h_0 W/f = 0{\cdot}24$. Note the poleward displacement of cyclones, the equatorward displacement of anticyclones, and the westward tilt of the eddy axes.

If the system imports no x momentum from the boundaries then the action of the Reynolds stress is to import momentum from the unforced latitudes, and the integrated momentum deficit over these defines the average jet strength over the forcing latitudes:

$$\begin{aligned}\langle \bar{u} \rangle &= \lambda^{-1}\overline{[v'u']}_{\infty}^{y_1} y_1^{-1} \\ &= \tfrac{1}{2} lk |A|^2 e^{-2dy_1} y_1^{-1} \lambda^{-1},\end{aligned} \tag{3.10}$$

always positive, i.e. westerly.

3.2. *Jet structure for topographic and source-sink forcing*

A solution to (3.5) in $-y_1 < y < y_1$ which matches ψ and ψ_y at the boundaries $y = \pm y_1$ with (3.6) is

$$C\{\cos Ly + iL\, e^{i(l+id)y_1}(l+id)^{-1}\cos(l+id)\, y\} \tag{3.11}$$

where

$$C = F\gamma k^2[\gamma^2(L^2 - l_0^2)^2 + \mu^2(L^2+k^2)^2]^{-\frac{1}{2}} e^{i\theta}$$

and

$$\theta = \arctan[-\mu(L^2+k^2)(L^2-l_0^2)^{-1}\gamma^{-1}]$$

with γ, μ, l, d, l_0 as defined by (3.7) *et seq.* and (3.8). Then in terms of the forcing constant

$$A = iCL(l+id)^{-1}\cos(l+id)\, y_1 \tag{3.12}$$

in the inviscid limit when $\mu = 0$, $d = 0$,

$$C(\mu = 0) = Fk^2(l^2 - L^2)^{-1}. \tag{3.13}$$

Substitution in (2.9), (2.17), (2.18), (3.3) and (3.4) then yields $\overline{u}(y)$ profiles. Examples are given in figure 3. For these k, L, H_0, f, $\bar{q}_y$ and W are each unity and $\mu = 0{\cdot}1$. Figures 4 and 5 show the dependence of $\overline{u}$ upon γ both at the axis and at the edge of the forcing region, $y = y_1 \equiv \Pi/2L$, for μ values of 10^{-3} and 10^{-1}.

As predicted the jet is invariably westerly when forced non-topographically and falls to low strength beyond the free Rossby-mode regime $-1 < \gamma < 0$. μ exerts a strong effect and with weak damping the jet achieves maximum strength both near $\gamma = 0$ and $\gamma = -1$. With topographic forcing the jet takes the direction of the forcing phase speed, and is strongest when this speed is near to the maximum for free Rossby modes, i.e. $c = -\bar{q}_y/k^2$; μ is influential only near to this maximum.

The structure of the net disturbance motion can be appreciated from a sketch of the stream function, figure 6. Conditions are those of curve A of figure 3 and on the plot the eddy stream function (3.11) has been combined with the resulting mean flow with a forcing velocity scale of 0·24. The mean westerly tilt implies a convergence of westerly momentum while the presence of the jet causes a poleward displacement of the cyclones and an equatorward displacement of the anticyclones, with unconnected westerly jets between them.

3.3. *Finite-amplitude effects*

Apart from harmonic terms, the effects of finite eddy amplitude appear through the influence of induced mean motion on apparent eddy phase speed or forcing frequency. Inclusion of an advection term $\overline{u}q'_x$ in (3.1) changes c to $c_a = (c-u)$; $\bar{q}_y$ becomes $(\bar{q}_y - u_{yy})$ and λ is also weakly modified.

By inspection of the $\overline{u}(\gamma)$ relation (figures 4 and 5) some general deductions can be made concerning the limits imposed by these effects when forcing is sufficiently strong. For example, if the forcing has a westward phase speed (i.e. $c < 0$) the presence of an easterly jet (as always occurs at the edge of the forcing region, and throughout it if forcing is topographic) reduces c_a and the apparent γ.

For topographic forcing the strong peak in forcing efficiency at $\gamma = -1$ implies that for $\gamma < -1$ the jet will have a limiting maximum speed of $(c + \bar{q}_y k^{-2})$, while for $-1 < \gamma < 0$ its speed will be somewhat less than c but in the same direction. For the easterly edge jets (however forced) the same effects apply, in addition to which the abrupt increase in d as γ (apparent) increases through zero (see figure 2) causes conditions close to critical layer absorption by enhancing the absorption of eddy momentum when the jet is strongest and resulting in a strengthening and narrowing of these jets, and a weakening of eddy amplitude beyond them.

A westerly jet, forced non-topographically by a strong westwards-travelling disturbance will accelerate until c_a falls below $-\bar{q}_y/k^2$, and will thus be limited in strength to about $\bar{q}_y/k^2 + c$.† These limits are compared with experimental results on figures 8 and 12.

† Another implication is that if a westerly jet exists over the forcing region, it will be sustained even if c is subsequently reduced to zero, so that the forcing pattern is stationary. Experiments more recent than are reported here qualitatively confirm this prediction.

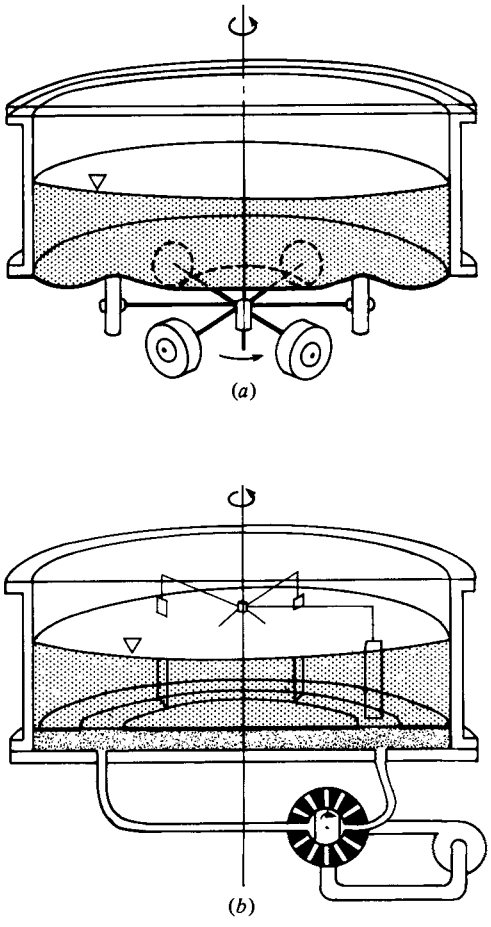

FIGURE 7. Experimental configurations: (*a*) Topographic forcing; (*b*) source–sink forcing, showing one of the mean flow measuring rotors over the forcing region, as used for one result series.

4. Experiments

Experiments were conducted with two configurations. The first employed topographic forcing in a cylindrical container. It was discovered that this was incapable of producing a significant westerly flow (see § 2.2) and some time later the apparatus was rebuilt to provide source–sink forcing through a porous bottom.

4.1. *Topographic-forcing configuration*

Reference is made to figure 7 (*a*). A cylindrical vessel 214 mm radius and 172 mm depth was mounted on a laboratory turntable. The bottom was made of a 1·2 mm thick rubber membrane against which there pressed at a pitch radius of 127 mm a set of six tangentially facing rollers mounted on a frame. A rigid disk supported the centre of the membrane. The roller frame could be rotated in either direction to cause

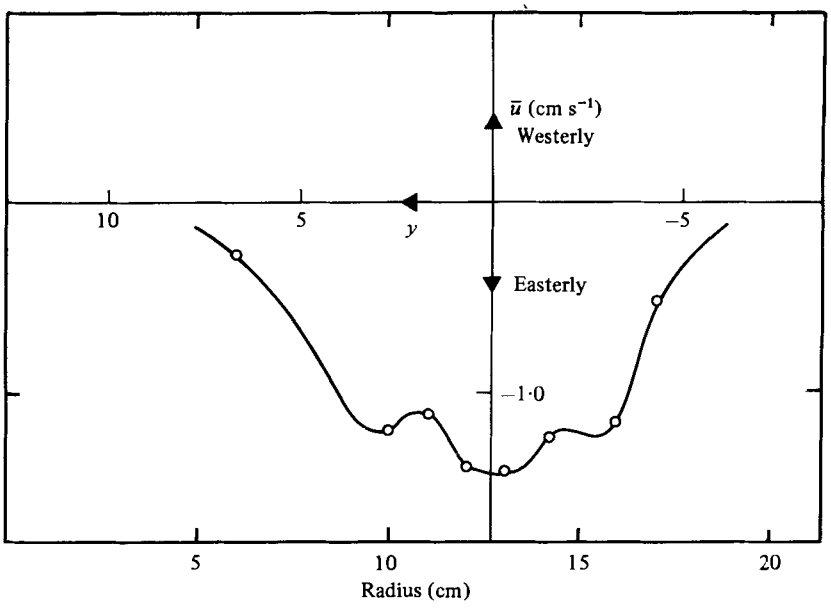

FIGURE 8. Measured radial structure of zonal mean flow, topographic forcing, $\gamma = 1{\cdot}53$; experimental conditions are given in text.

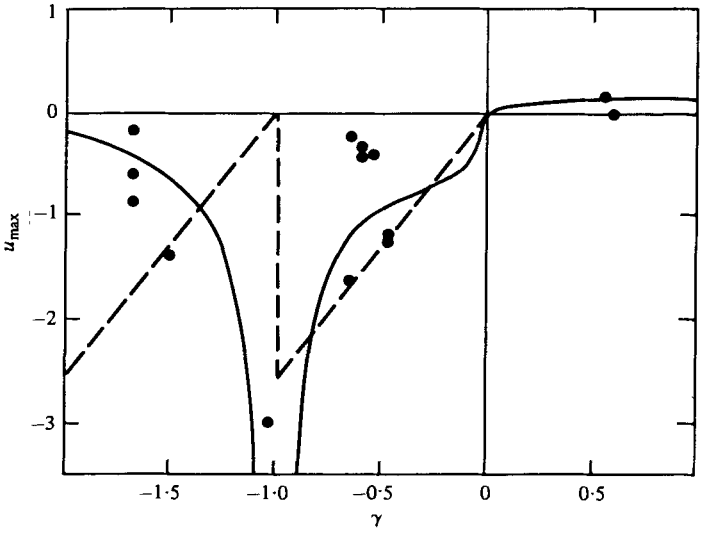

FIGURE 9. Topographic forcing: experimental and theoretical results compared. For conditions see text. Points are experimental $\bar{u}(y)$ maxima. Solid line is the theoretical $\bar{u}(y = 0)$ neglecting Doppler corrections to forcing frequency. Broken line is the limit to $\bar{u}$ for an inviscid medium, imposed by Doppler shift of forcing frequency (see §3.3).

a wavelike bottom disturbance of about ± 4 mm amplitude and zonal wavenumber six to move around the bottom.

The vessel was filled to a depth of about 60 mm with thin silicone oil and the whole assembly was rotated axially causing the free surface to deform centrifugally to give $\bar{q}_y > 0$ with y measured radially inward. The motion of surface particles was observed

by a television camera mounted on the turntable. Mean velocities were derived from the time required for particles within a given annular sector to travel twenty degrees. The measurement was therefore quasi-Lagrangian, but further refinement of technique was not considered worthwhile at the time.

Quantitative results were taken in only one experimental sequence. For these, $h_0 = 52\,\text{mm}, f = 9{\cdot}72\,\text{s}^{-1}$ and $h' = 4\,\text{mm}$. Hence $\bar{q}_y(y = 0) = 0{\cdot}057\,\text{mm}^{-1}\,\text{s}^{-1}, H = 0{\cdot}077$, $\mu = 0{\cdot}035$.

Figure 8 shows the radial structure for $\gamma = -1{\cdot}53$. The mean flow is easterly everywhere but is broader and much stronger than predicted theoretically, and exhibits much more pronounced weakening at its edges. These features and the suggestion of trimodality in the jet are consistent with a reduction in apparent phase speed as outlined in § 3.3.

Figure 9 compares observed jet maxima with theory (solid line) as a function of γ. Also shown is the finite amplitude inviscid limit (broken line) defined in § 3.3.

The scatter in the data is unexplained, but may reflect the possibility of multiple values in terminal jet strength. Such as they are the results show a mean flow in the direction of forcing, a maximum strength comparable to the inviscid predicted maximum and departing from the small-amplitude prediction in a manner consistent with first-order finite amplitude effects.

4.2. *Source–sink forcing configuration*

Referring to figure 7 (*b*), the vessel was inverted and its bottom was perforated by 36 equally spaced holes at a radius of 142 mm. Each hole connected by nylon hydraulic tubing to a 'fluid commutator', a manifold containing a rotatable, ported centre-body. Fluid pumped to the commutator produced a cyclic flow through the tubes to create a pattern of sources and sinks on the tank bottom with an azimuthal wavenumber of 6. Rotation of the centre-body caused the pattern to move 'east' or 'west'. A p.v.c. foam sheet lay over the bottom to diffuse the jets and flow was confined with an annulus 164 mm outer radius and 121 mm radius, by sealing the remainder of the foam surface with thick paint.

The vessel was filled to about 60 mm depth with water and the motion of slightly buoyant polystyrene beads was photographed from above and observed by television camera. Results were obtained mainly by the laborious process of digitizing the coordinates of particle streaks within 60 degree sectors in the photograph sequences, and then computing $\bar{u}$ and $(\overline{u'v'})$ profiles. For one data set (appearing on figure 12) however, a pair of very light five-armed rotors was suspended in the water, free to turn about a vertical central axis, as shown sectioned in figure 7 (*b*). These rotors had blades 10 mm wide and lay at 116 and 142 mm radius. With these, the approximate Eulerian mean azimuthal velocities could be measured directly from the television monitor.

Figures 10 (*a*) and 10 (*b*) (plates 1 and 2) show half-second time exposures of surface particle movement under eastward ($\gamma = +0{\cdot}36$) and westward ($\gamma = -0{\cdot}36$) forcing conditions respectively. Background rotation is clockwise. For these tests $f = 8{\cdot}46\,\text{s}^{-1}$, $h_0 = 5{\cdot}8\,\text{cm}$, $\bar{q}_y(y = 0) = 0{\cdot}38\,\text{cm}^{-1}\,\text{s}^{-1}$, and $k = 0{\cdot}42\,\text{cm}^{-1}$. By direct measurement $W'_{0\text{max}} = 0{\cdot}2\,\text{cm}\,\text{s}^{-1}$, and over the forcing region $\lambda \simeq 0{\cdot}115\,\text{s}^{-1}$. With westward forcing the presence of a westerly jet is made evident by the relative inward radial displacement of the cyclones and outward displacement of the anticyclones (cf.

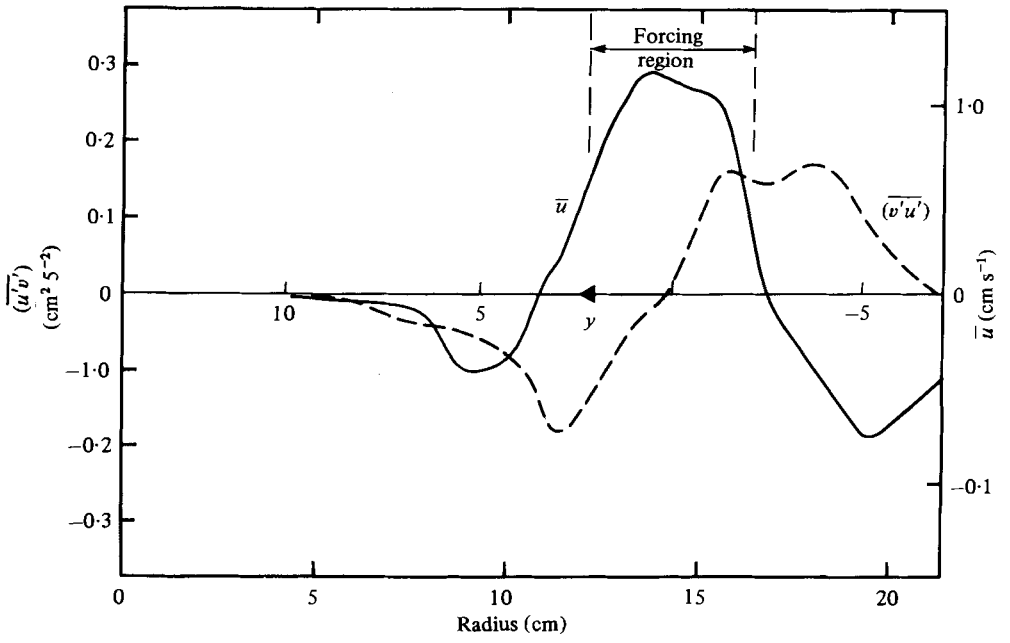

FIGURE 11. Mean velocity and Reynolds stress profiles, source–sink forcing, $f = 9{\cdot}74$ s^{-1}; $h_0(y = 0) = 7{\cdot}4$ cm s^{-1}; $W'_{0\max} = 0{\cdot}2$ cm s^{-1}, $\gamma = -0{\cdot}37$.

figure 6). An easterly boundary jet is more clearly discernible on the inside of the forcing region, and it will be noted that inside the jet the particle movements are very small, implying a strong absorption of the eddies by this jet (see § 3.3).

With eastward forcing the eddies are somewhat weaker and more constant in radial position. The cyclones are discernably stronger than the anticyclones, implying the presence of a cyclonic shear over the forcing region. The inner boundary jet is still evident, but the eddy motion inside it is greater than in the westerly-forcing case.

Using digitized co-ordinates of particle streaks within sixty degree sectors in photograph sequences, the Eulerian mean azimuthal velocity and mean-Reynolds-stress distribution were computed. Figure 11 gives the $\bar{u}$ and $\overline{u'v'}$ for an experiment in which $f = 9{\cdot}74$ s^{-1}, $h_0(y = 0) = 7{\cdot}4$ cm, $\gamma = -0{\cdot}37$, $W_{0\max} = 0{\cdot}2$ cm s^{-1}. A parabolic filter of 3 cm radial width has been applied to smooth the results.

There is good qualitative correspondence between zeros and maxima in $\bar{u}$ and $(\overline{u'v'})_y$, and if the values of $(\overline{u'v'})_y$ at 12·5, 14·8 and 19·5 cm are substituted in (2.18) with values of $\bar{u}$ maxima at 14·0 and 19·5 the value of λ so given is between 0·08 s^{-1} and 0·10 s^{-1}. This is in fair quantitative agreement with a λ estimated at between 0·065 s^{-1} and 0·09 s^{-1} by direct measurement of the spin-down of eddies over the forcing region after forcing has ceased.

Figure 12 shows the measured dependence of $\bar{u}$ at $r = 14{\cdot}25$ cm (i.e. $y = 0$, over the forcing axis) and $r = 11{\cdot}6$ cm ($y = 2{\cdot}65$ cm, beyond the edge of the forcing region at 2·15 cm) as a function of γ for a fixed $f = 8{\cdot}46$ s^{-1}, $h_0 = 5{\cdot}76$ cm and $W_{0\max} = 0{\cdot}2$ cm s^{-1}. The $y = 0$ results are from the sequence that included figures 9 and 10, and also from a separate sequence using the drift measuring rotor described above.

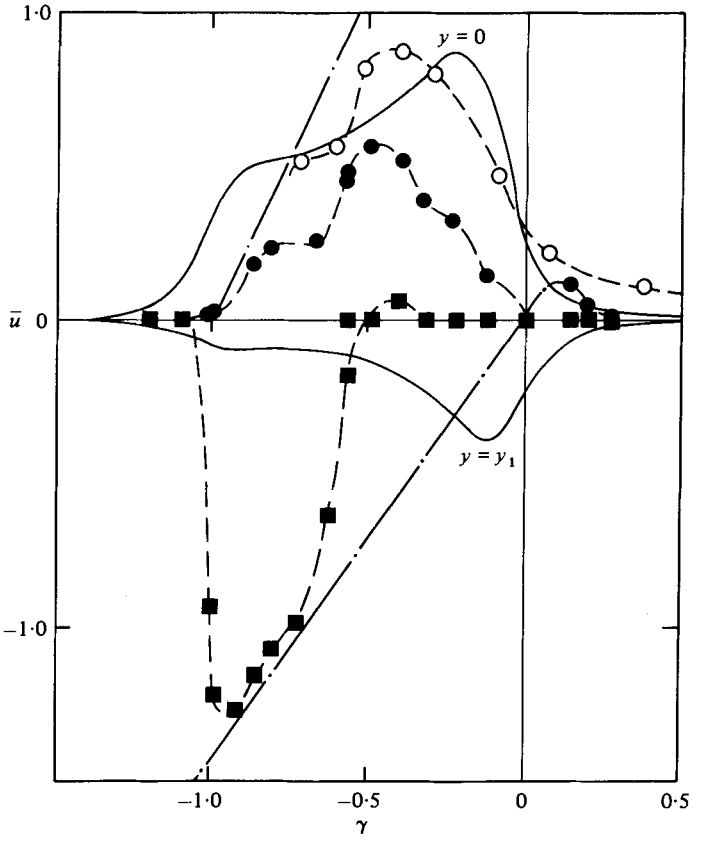

FIGURE 12. Mean-flow dependence on forcing phase speed, source–sink forcing. For conditions see text. ○, $\bar{u}(-0{\cdot}5 < y < 0{\cdot}5$ cm) by photo analysis. ●, $\bar{u}(-0{\cdot}5 < y < 0{\cdot}5$ cm) by rotor measurement. ■, $\bar{u}(y = 2{\cdot}65$ cm). ——, linear theory. – – –, phase-speed limits.

Although their form is similar, the rotor measurements yield a lower $\bar{u}$, perhaps due to the interruption of the eddies by the rotor blades. The $y = 2{\cdot}65$ cm results came from rotor measurements alone. Friction evidently prevented movement at very low drift rates. Also presented (solid lines) are theoretical curves of $u(\gamma)$ for $y = 0$ and $y = 2{\cdot}65$ cm predicted using the equations of § 3.2, and the limits imposed by Doppler shift of the apparent phase speed as discussed in § 3.3. The theoretical curves have been normalized to give the same maximum $\bar{u}$ $(y = 0)$ as the photo results, and correspond to a $W_{0\max}$ of 0·12 cm s^{-1}.

The experimental results always lie within the Doppler limits, and on the axis at least bear a crude similarity to the theory. It is evident however that Doppler-shifting alone is insufficient to explain the discrepancies (that effect being to shift the theoretical curves rightward an amount $\bar{u}k^2q_y$). In particular the strong easterly boundary jet suggests important wave-momentum absorption effects not accommodated in the present theory. Other effects likely to influence a quantitative comparison are the bounded circular geometry and spatial non-uniformity in $\bar{q}_y$, h_0 and λ.

5. Conclusion

The experiments have provided a useful confirmation of the major predictions of quasi-geostrophic theory for the eddy forcing of mean flows in the presence of a gradient of mean potential vorticity. In particular it is demonstrated that if the eddies are steadily forced at a localized latitude, the forcing region will be bounded by easterly jets whose strength is determined by the viscous spin-down time scale and the divergence of eddy Reynolds stress.

Within the forcing latitudes the character of the mean flow is dependent upon the nature of the forcing, and it is shown and experimentally verified that a topographic deformation of the vorticity field is ineffectual because to highest order the mean flow forcing is balanced completely by topographic drag; the mean flow then derives from the effect of viscous spin-down on the eddies, and takes the direction of phase propagation of the disturbance.

Non-topographic forcing can generate intense westerly jets whose strength can approach the phase-speed of the eddies forcing them; the kinematical effect is a poleward displacement of the cyclones and an equatorward displacement of the anticyclones. For any generation process which does not impart mean momentum to the flow, the jet over the forcing region is always westerly; for the present configuration its strength and the strength of the bounding easterly jets falls abruptly as the forcing phase speed c passes beyond the range $-0{\cdot}1 < ck^2/\bar{q}_y < 0$ for inviscid free barotropic modes.

Although qualitatively in agreement, the detailed correspondence between the experiments and the linear theory presented in § 3 leaves a lot to be desired. Insofar as the induced flows were comparable in strength to the phase-speed of the forcing disturbances, and their vorticities and vorticity gradients were of similar magnitude to the background, it is likely that Doppler-shifting and other nonlinear effects would be appreciable. In particular the inordinate strength of the easterly boundary jet with source–sink forcing (figure 12) reveals the likely occurrence of enhanced absorption of the eddies by the induced mean flow in regions where the Doppler-shifted phase speed is reduced.

The assistance of Terry Long (Monash University) and George Scott is gratefully acknowledged. The topographic forcing experiments were done in the Geophysical Fluid Dynamics Laboratory at Monash University.

REFERENCES

ANDREWS, D. G. & MCINTYRE, M. E. 1978 An exact theory of nonlinear waves on a Lagrangian-mean flow. *J. Fluid Mech.* **89**, 609–646.

BAINES, P. G. & FREDERIKSEN, J. S. 1978 Baroclinic instability on a sphere in two-layer models. *Quart. J. Roy. Met. Soc.* **104**, 45–68.

BLACKMON, M. L., WALLACE, J. M., LAU, N. & MULLEN, S. L. 1977 An observational study of the Northern Hemisphere wintertime circulation. *J. Atmos. Sci.* **34**, 1040–1053.

COLIN DE VERDIÈRE, A. 1977 Quasi-geostrophic flows and turbulence in a rotating homogeneous fluid. Ph.D. thesis, Woods Hole Oceanographic Institution, Massachusetts.

COLIN DE VERDIÈRE, A. 1979 Mean flow generation by topographic Rossby waves. *J. Fluid Mech.* **94**, 39–64.

FREDERIKSEN, J. S. 1979 The effect of long planetary waves on the regions of cyclogenesis: linear theory. *J. Atmos. Sci.* **36**, 195–204.

HELD, I. M. 1975 Momentum transport by quasi-geostrophic eddies. *J. Atmos. Sci.* **32**, 1494–1497.

HOLOPAINEN, E. O. 1978 On the dynamic forcing of the long-term mean flow by the large-scale Reynolds stresses in the atmosphere. *J. Atmos. Sci.* **35**, 1596–1604.

HOLLINGSWORTH, A. 1975 Baroclinic instability of simple flow on a sphere. *Quart. J. Roy. Met. Soc.* **101**, 495–528.

LORENZ, E. N. 1960 Energy and numerical weather prediction. *Tellus* **12**, 364–373.

MCINTYRE, M. E. 1980 An introduction to the generalised Lagrangian-mean description of wave, mean-flow interaction. *Pageoph.* **118**, 152–176.

MOURA, A. D. & STONE, P. H. 1976 The effects of spherical geometry on baroclinic instability. *J. Atmos. Sci.* **33**, 602–616.

NEWELL, R. E., KIDSON, J. W., VINCENT, D. G. & BOER, G. J. 1972 *The General Circulation of the Tropical Atmosphere and Interactions with Extratropical Latitudes.* Massachusetts Institute of Technology Press.

OORT, A. & RASMUSSEN, E. M. 1971 Atmospheric circulation statistics. *N.O.A.A. Prof. Paper* 5. U.S. Govt. Printing Office.

RHINES, P. B. 1977 The dynamics of unsteady currents. *The Sea*, vol. 6 (ed. E. D. Goldberg, I. N. McCave, J. J. O'Brien & J. H. Stelle), pp. 189–318. Wiley.

RHINES, P. B. & HOLLAND, W. R. 1979 A theoretical discussion of eddy-driven mean flows. *Dyn. of Atmospheres & Oceans* **3**, 289–325.

SIMMONS, A. J. & HOSKINS, B. J. 1976 Baroclinic instability on the sphere: normal modes of the primitive and quasi-geostrophic equations. *J. Atmos. Sci.* **33**, 1454–1477.

STARR, V. P. 1968 *Physics of Negative Viscosity Phenomena.* McGraw-Hill.

STERN, M. E. 1975 *Ocean Circulation Physics.* Academic.

TAYLOR, G. I. 1915 Eddy motion in the atmosphere. *Phil. Trans. Roy. Soc.* A **15**, 1–26.

THOMPSON, R. O. R. Y. 1971 Why there is an intense Eastward current in the North Atlantic, but not in the South Atlantic. *J. Phys. Oceanog.* **1**, 235–237.

THOMPSON, R. O. R. Y. 1977 Observations of Rossby waves near Site D. *Prog. Oceanog.* **7**, 135–162.

THOMPSON, R. O. R. Y. 1978 Reynolds stress and deep counter currents near the Gulf Stream. *J. Mar. Res.* **36**, 611–615.

WEBSTER, F. 1965 Measurements of the eddy fluxes of momentum in the surface layer of the Gulf Stream. *Tellus* **17**, 239–245.

WHITEHEAD, J. 1975 Mean flow generated by circulation on a β-plane: an analogy with the moving flame experiment. *Tellus* **27**, 358–364.

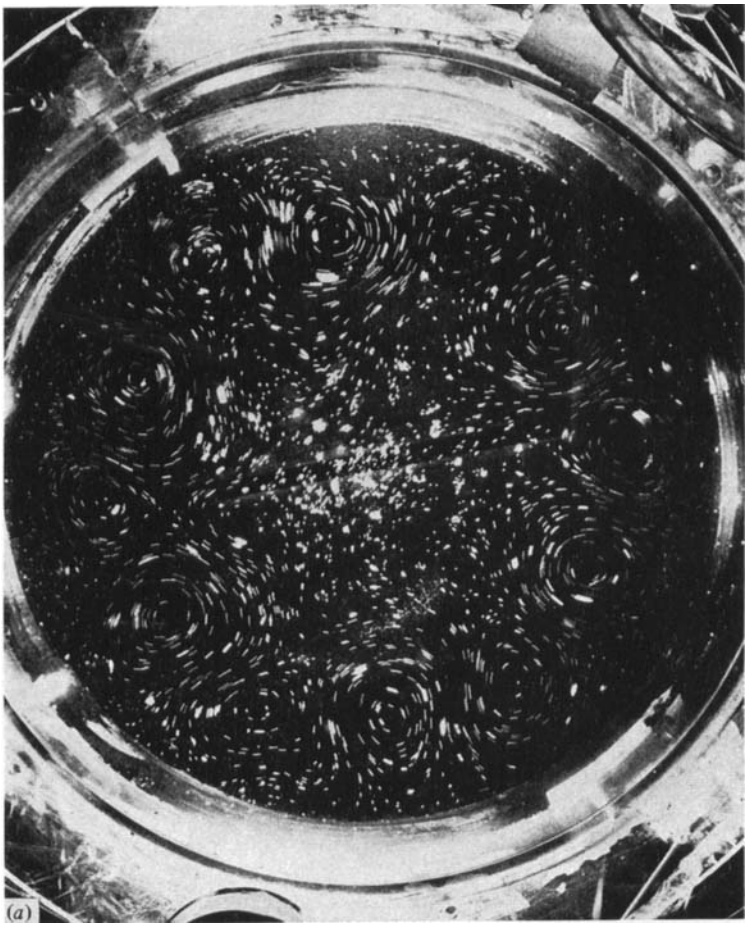

FIGURE 10. Movement of surface particles. Half-second exposures, clockwise background rotation; $f = 8{\cdot}46\ \mathrm{s}^{-1}$, $h_0 = 5{\cdot}8$ cm, $\bar{q}(y = 0) = 0{\cdot}38\ \mathrm{cm}^{-1}\ \mathrm{s}^{-1}$, $k(y = 0) = 0{\cdot}42\ \mathrm{s}^{-1}$, $W'_{\max} = 0{\cdot}2$ cm s^{-1}. (*a*) Eastward forcing, $\gamma = 0{\cdot}36$. (*b*) Westward forcing $\gamma = -0{\cdot}36$.

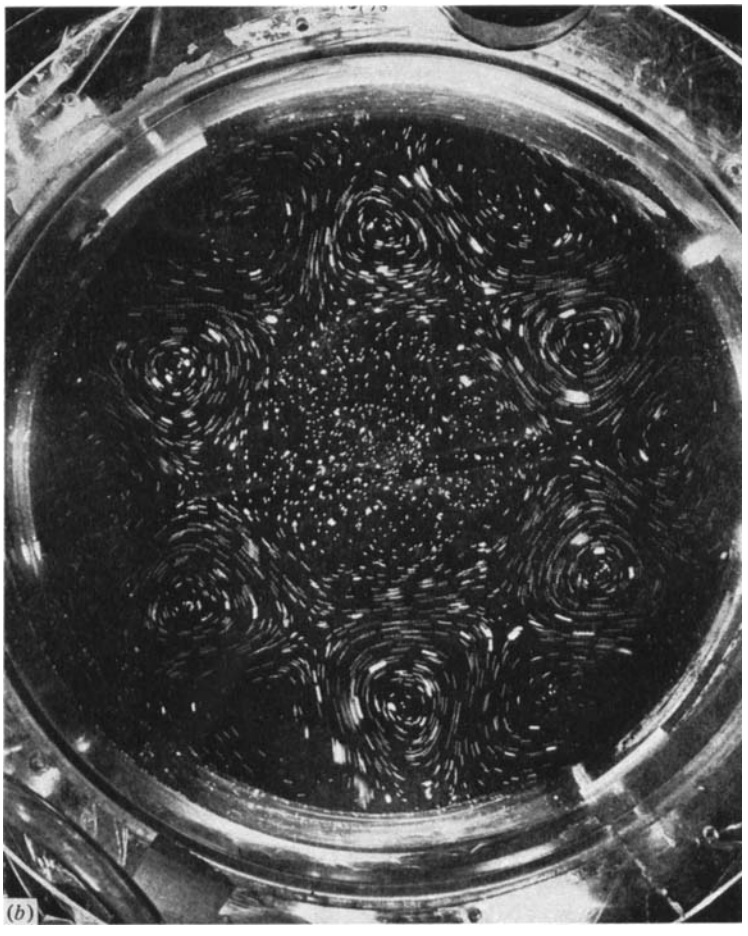

FIGURE 10 (*b*). For legend see plate 1.